The Wannier function approach to photonic crystal circuits

2003 J. Phys.: Condens. Matter 15 R1233

(http://iopscience.iop.org/0953-8984/15/30/201)

INSTITUTE OF PHYSICS PUBLISHING JOURNAL OF PHYSICS: CONDENSED MATTER

J. Phys.: Condens. Matter **15** (2003) R1233–R1256 PII: S0953-8984(03)36570-1

TOPICAL REVIEW

The Wannier function approach to photonic crystal circuits

Kurt Busch[1,4], **Sergei F Mingaleev**[1,2], **Antonio Garcia-Martin**[1,3], **Matthias Schillinger**[1] **and Daniel Hermann**[1]

[1] Institut für Theorie der Kondensierten Materie, Universität Karlsruhe, 76128 Karlsruhe, Germany
[2] Bogolyubov Institute for Theoretical Physics, 03143 Kiev, Ukraine
[3] Instituto de Microelectronica de Madrid, Consejo Superior de Investigaciones Cientificas, Isaac Newton, 8 (PTM), 28760-Tres Cantos, Madrid, Spain

E-mail: kurt@tkm.physik.uni-karlsruhe.de

Received 10 April 2003
Published 18 July 2003
Online at stacks.iop.org/JPhysCM/15/R1233

Abstract

We introduce a novel approach to the accurate and efficient calculation of the optical properties of defect structures embedded in photonic crystals (PCs). This approach is based on an expansion of the electromagnetic field into optimally adapted photonic Wannier functions, which leads to effective lattice models of the PC structures. Calculations for eigenmode frequencies of simple and complex cavities as well as the dispersion relations for straight waveguides agree extremely well with the results from numerically exact supercell calculations. Similarly, calculations of the transmission through various waveguiding structures agree very well with the results of corresponding finite-difference time domain simulations. Besides being substantially more efficient than standard simulation tools, the Wannier function approach offers considerable insight into the nature of defect modes in PCs. With this approach, design studies and accurate simulation of optical anisotropic and non-linear defects as well as detailed investigations of disorder effects in higher-dimensional PCs become accessible.

(Some figures in this article are in colour only in the electronic version)

Contents

[4] Author to whom any correspondence should be addressed.

1. Introduction

During the last few years optical fibres have started to replace electrical wires in short-distance communications such as in local area networks and computer-to-computer links. However, the realization of a completely seamless, all-optical network, where information processing as well as communication would take place with laser light rather than electricity, requires novel optical materials capable of trapping and micro-moulding the flow of light. This is because the light in an optical fibre easily escapes into the background electromagnetic modes of empty space if the fibre is bent or distorted on a microscopic scale.

Photonic crystals (PCs) represent a novel class of optical materials which facilitate the realization of such an integrated photonics. In these periodic dielectric structures, a carefully engineered combination of microscopic scattering resonances from individual elements of the periodic array and Bragg scattering from the corresponding lattice leads to the formation of a photonic band structure. In particular, the flexibility in material composition, lattice periodicity, symmetry, and topology allows one to tailor the photonic dispersion relations to almost any application need. The most dramatic modification of the photonic dispersion in these systems occurs when suitably engineered PCs exhibit frequency ranges over which the propagation of light is forbidden regardless of direction [1–3]. The existence of these so-called complete photonic band gaps (PBGs) allows one to eliminate the problem of light leakage from sharply bent optical fibres. Indeed, using a PC with a complete PBG as a background material and embedding into this PC a circuit of properly engineered waveguiding channels permits the creation of an optical micro-circuit inside a perfect optical insulator, i.e. a close analogue of customary electronic circuits.

These prospects have triggered enormous experimental activities aimed at the fabrication of two-dimensional (2D) and three-dimensional (3D) PC structures for telecommunication applications with PBGs in the near-infrared frequency range. Considering that the first Bragg resonance occurs when the lattice constant equals half the wavelength of light, fabrication of PCs with band gaps in the near IR requires substantial technological resources. For 2D PCs, advanced planar microstructuring techniques borrowed from semiconductor technology can greatly simplify the fabrication process, and high-quality PCs with embedded defects and waveguides have been fabricated in various material systems such as semiconductors [4–9], polymers [10, 11], and glasses [12, 13]. In these structures, light experiences PBG effects in the plane of propagation, while the confinement in the third direction is achieved through index guiding. This suggests that fabricational imperfections in bulk 2D PCs as well as deliberately embedded defect structures such as cavities and waveguide bends in 2D PCs will inevitably lead to radiation losses into the third direction. Therefore, it is still an open question whether devices with acceptable radiation losses [14] can be designed and realized in 2D PCs. However, radiation losses can be avoided altogether if light is guided within the complete PBGs of 3D PCs and, therefore, the past years have seen substantial efforts towards the manufacturing of suitable 3D PCs. These structures include layer-by-layer structures [15, 16],

inverse opals [17–19], as well as the fabrication of templates via laser holography [20, 21] and two-photon polymerization [22–24]. Given this tremendous flexibility in the fabrication of PCs, it is clear that any experimental exploration, or technological exploitation, of PCs has to be accompanied by a quantitative theoretical analysis. Detailed numerical simulations of PC structures allow one to interpret experimental data and help to extract relevant parameters. Perhaps more importantly, the theoretical design of PC structures allows one to identify the most interesting cases and to investigate stable designs for successfully operating devices.

To date, theoretical investigations of defect structures in PCs have almost exclusively been carried out by employing finite-difference time domain (FDTD) discretizations of Maxwell's equations [25]. These general-purpose techniques for the simulation of arbitrary dielectric and metallic structures are well known in the electrical engineering community and have been perfected over some 30 years. However, the generality of the FDTD approach, while allowing its application to arbitrary defect structures, at the same time puts severe constraints on its usefulness for the design of PC circuits. Typical FDTD computations require a minimum of 10 grid points per wavelength for each spatial dimension, so simulations of large PC structures lead to formidable requirements on computational resources. Moreover, the low group velocities near photonic band edges, and for certain waveguiding modes, imply that corresponding simulation times for PC structures are considerably longer than those in traditional high-index waveguiding systems.

The computational effort required for solving partial differential equations (PDEs) can be substantially reduced by employing Galerkin-type methods [26], which rely on an expansion of the solution into an orthogonal set of basis functions. The efficiency of this approach depends crucially on the choice of an appropriate basis set. For instance, extended plane waves are ill-suited to describe localized defect modes in PCs because accurate calculations of simple defect structures already require several thousands of plane waves. As a consequence, plane-wave expansions, in the form of supercell calculations, are of practical importance only for the design of simple cavities and straight waveguides as well as for gauging more advanced methods. A more natural expansion basis for defect modes in PCs consists in an orthogonal set of localized functions such as Hermite–Gaussian functions, and the corresponding technique has been pioneered by Mogilevtsev *et al* [27]. Despite providing certain improvements over plane-wave expansions, the localized function method [27] still requires several hundreds of basis functions for obtaining accurate results and is, therefore, restricted to applications involving few defects as, for instance, in the design of PC fibres [28, 29].

The heavy numerical load associated with FDTD, finite-element (FE), and standard Galerkin-type simulations of defect structures in PCs may be directly traced to the fact that these approaches disregard any information about the underlying PC structure. However, this information is readily available from standard photonic band-structure computation, which provides dispersion relations and associated mode structures for infinitely extended, perfectly periodic PCs. In particular, the eigenmodes of a given PC, the Bloch functions, constitute a natural and complete basis set of functions that have encoded into them all the information of the corresponding PC. The extended nature of Bloch functions, however, makes them less suited for the expansion of localized defect modes.

Therefore, a number of authors have recently set out to adapt the *tight-binding approximation* [30] of electronic structure theory to PCs [31–33]. In such an approach, the Bloch functions are expanded into a set of 'atomic orbitals' and the expansion parameters are determined by fitting the resulting band structure to *ab initio* calculations. Once these approximate Bloch functions have been obtained, a localized basis set can be generated by means of a lattice Fourier transform. However, the success of empirical tight-binding parametrizations depends crucially on the existence of appropriate localized 'orbitals' of the

individual 'atoms' that make up the crystal [34, 35]. As a consequence, the adaptation to PCs presents major problems because bound states for a single dielectric scatterer simply do not exist and until now no tight-binding parametrization for TE-polarized radiation in 2D PCs or electromagnetic waves in 3D PCs has been obtained. This has led a number of authors to base a tight-binding approximation on an expansion into modes associated with a single cavity defect [36–39]. While this is a perfectly legitimate approximation, its application is limited in the sense that it requires the existence of a complete PBG in the underlying PC to obtain localized expansion functions via supercell calculations. Furthermore, there does not appear to be a straightforward way to systematically improve upon the initial approximation by incorporating additional, higher-order cavity modes as, in most instances, the latter do not exist. Nevertheless, this approach provides a physically intuitive picture of wave propagation through defect structures in PCs.

An alternative route to the construction of *approximate* lattice models starts from the Lippmann–Schwinger equation for electromagnetic radiation in PCs and utilizes an expansion of the electromagnetic field into localized functions centred at PC lattice sites [40, 41]. Within this approach, knowledge of the underlying PC is contained in the Green function of the perfect lattice which may be calculated from the photonic Bloch functions. A careful analysis of the decay properties of the Green function with increasing separation of its two spatial arguments reveals that the construction of lattice models for PCs requires one to go beyond nearest-neighbour interaction [41–43, 53], which may lead to novel phenomena such as stable solitonic excitations in non-linear 2D PCs [42, 43]. However, to date, only monopole-type defect modes can be considered in this approximation and the inclusion of higher-order multipole-type defect modes is not straightforward.

In this review, we introduce a novel approach to the calculation of the optical properties of defect structures embedded in PCs. This approach is based on an expansion of the electromagnetic field into optimally adapted *photonic Wannier functions* which are calculated directly from the Bloch functions without going through a tight-binding parametrization. As a consequence, we obtain a lattice model with more than nearest-neighbour interaction whose accuracy can be systematically improved by adding additional Wannier functions for higher bands. The Wannier function approach was developed in the context of electronic problems in 1937 [44], and has proven its usefulness as a starting point for various formal developments such as the semiclassical theory of electron dynamics and the theory of magnetic interactions in solids. In 1993 Leung [45] suggested that the Wannier function approach should be very efficient in investigating the properties of PCs. Since then, the formal existence of an orthonormal basis of localized Wannier functions has been used [31–33, 36–39] to justify the tight-binding approximation which we discussed above. However, until now the *practical* importance of the Wannier function approach has been fairly minimal because of the difficulties involved in calculating well-localized Wannier functions.

The situation changed dramatically after the publication by Marzari and Vanderbilt of a new method for calculating *maximally localized* generalized Wannier functions in crystalline solids [46]. Quite recently this method has been extended to the case of 2D PCs [47–49] and the efficiency of using the photonic Wannier functions for calculations of simple defect cavities has been demonstrated [47, 48]. Here, we systematically describe how the maximally localized photonic Wannier functions can be calculated, and demonstrate how they can be efficiently used for various applications, such as determining the transmission properties of PC circuits. In particular, we point out that the computational efficiency of the Wannier function approach is comparable (and even exceeds) the efficiency of multiple-multipole methods, based on using such specialized functions as cylindrical [50, 51] or vector spherical [52] harmonics, which are currently believed to be the most efficient methods for calculations for PC structures made

of *ideally spherical* or *cylindrical* scatterers (see the discussion at the end of section 4.3). Besides this, in contrast to the multiple-multipole methods, the Wannier function approach can be applied to PCs with arbitrary shapes of individual scatterers.

The review is organized as follows. In section 2, we review photonic band-structure computation, which lies at the heart of our Wannier function approach. The calculation of optimally localized Wannier functions from photonic Bloch functions is discussed in section 3. These Wannier functions facilitate the construction of lattice models for PCs as discussed in section 4. Based on this, the accuracy and efficiency of the Wannier function approach is demonstrated through detailed calculations of cavity modes in section 4.1. Further illustrations include the determination of waveguide dispersion relations in section 4.2 and calculations of the transmission through bends in section 4.3. Finally, in section 5, we show how large-scale PC circuits can be simulated efficiently through combining a recently developed scattering matrix approach [54] with Wannier function simulations.

2. Photonic band-structure calculations

Virtually any theoretical investigation of PC defect structures starts with the computation of the photonic band structure associated with the infinitely extended, perfectly periodic underlying PCs. These computations permit the determination of dispersion relations and associated mode structures of perfect PCs. This allows us to identify PBGs and the symmetry properties of the modes. Other physical quantities of interest, such as the density of states, the local density of states [55], and the group velocity [56, 57], can be directly obtained from these calculations. In the present review, we restrict ourselves to the case of TM-polarized radiation propagating in 2D PCs, and in the following we discuss photonic band-structure computation for this case only. However, we would like to emphasize that the Wannier function approach can easily be extended to the description of TE-polarized radiation in 2D PCs as well as to the propagation of electromagnetic waves in 3D PCs.

The TM-polarized radiation that propagates in the (x, y) plane of a perfect 2D PC is most conveniently described through the z-component of the electric field, $E(\vec{r}, t)$, which obeys the wave equation

$$\left[\nabla^2 + \left(\frac{\omega}{c}\right)^2 \varepsilon_{\mathrm{p}}(\vec{r})\right] E(\vec{r}) = 0. \tag{1}$$

Here, we have assumed a time harmonic dependence, $E(\vec{r}, t) = \exp(-\mathrm{i}\omega t)E(\vec{r})$, of the electric field with the frequency, ω. In addition, c and $\vec{r} = (x, y)$ denote the vacuum speed of light and the in-plane position vector respectively, and $\nabla^2 = (\partial_x^2 + \partial_y^2)$ represents the 2D Laplacian. All the structural information of the PC is encoded into the dielectric constant, $\varepsilon_{\mathrm{p}}(\vec{r}) \equiv \varepsilon_{\mathrm{p}}(\vec{r} + \vec{R})$, which is periodic with respect to the set $\mathcal{R} = \{n_1\vec{a}_1 + n_2\vec{a}_2;\ (n_1, n_2) \in \mathcal{Z}^2\}$ of lattice vectors $\vec{R}$ that are generated by the primitive translations $\vec{a}_1$ and $\vec{a}_2$.

Since equation (1) is a PDE with periodic coefficients, its solutions obey the Bloch–Floquet theorem. This allows one to label the solutions with a wavevector $\vec{k}$, the so-called crystal momentum. Furthermore, restricting the wavevector, $\vec{k}$, to lying within the first Brillouin zone (BZ) [30], we introduce an integer index n, the so-called band index, labelling the solutions for a given wavevector, $\vec{k}$. Such solutions are commonly referred to as the Bloch functions, $E_{n\vec{k}}(\vec{r})$, of the underlying PC. They satisfy the Bloch–Floquet theorem

$$E_{n\vec{k}}(\vec{r} + \vec{R}) = \mathrm{e}^{\mathrm{i}\vec{k}\cdot\vec{R}} E_{n\vec{k}}(\vec{r}), \tag{2}$$

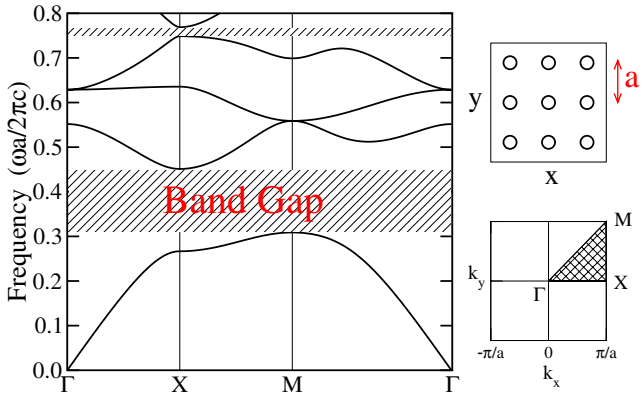

Figure 1. Photonic band structure for TM-polarized radiation in a square lattice (lattice constant a) of cylindrical dielectric rods (radius $r_{\mathrm{rod}} = 0.18a$ and $\varepsilon_{\mathrm{rod}} = 11.56$) in air. This PC exhibits a large fundamental gap extending from $\omega = 0.302 \times 2\pi c/a$ to $0.443 \times 2\pi c/a$. A higher-order band gap extends from $\omega = 0.738 \times 2\pi c/a$ to $0.763 \times 2\pi c/a$.

and represent a complete orthogonal set of functions:

$$\int_{\mathbb{R}^2} \mathrm{d}^2\vec{r}\; E^*_{n\vec{k}}(\vec{r})\varepsilon_{\mathrm{p}}(\vec{r})E^*_{n'\vec{k}'}(\vec{r}) = \delta_{nn'}\delta(\vec{k}-\vec{k}'), \tag{3}$$

where the integration runs over the entire space $\mathbb{R}^2$. The eigenfrequencies, $\omega_{n\vec{k}}$, belonging to the Bloch functions, $E_{n\vec{k}}(\vec{r})$, acquire the same composite label and may be represented in a band diagram.

A straightforward way of solving equation (1) is to expand all the periodic functions, $\exp(-\mathrm{i}\vec{k}\cdot\vec{r})E_{n\vec{k}}(\vec{r})$ and $\varepsilon_{\mathrm{p}}(\vec{r})$, into a Fourier series over the reciprocal lattice $\mathcal{G}$, thereby transforming the differential equation into an infinite-matrix eigenvalue problem, which may be suitably truncated and solved numerically. Details of this plane-wave method (PWM) for isotropic systems can be found, for instance, in [55, 58] and for anisotropic systems in [59].

While the PWM provides a straightforward approach to computing the band structure of PCs, it also exhibits a number of shortcomings, such as slow convergence associated with the truncation of Fourier series in the presence of discontinuous changes in the dielectric constant. Therefore, we have recently developed an efficient real-space approach to computing photonic band structures [57]. Within this approach, the wave equation (1) is discretized in real space through finite differences or more advanced FE techniques leading to sparse matrix problems. The solutions of the resulting algebraic problems are obtained by employing *multi-grid methods*, which guarantee an efficient solution by taking full advantage of the smoothness of the photonic Bloch functions. In figure 1, we show the band structure for TM-polarized radiation in a 2D PC consisting of a square lattice (lattice constant a) of cylindrical dielectric rods (radius $r_{\mathrm{rod}} = 0.18a$ and dielectric constant $\varepsilon_{\mathrm{rod}} = 11.56$) in air. This structure exhibits two complete band gaps. The larger, fundamental band gap (38%) extends between $\omega = 0.302 \times 2\pi c/a$ to $0.443 \times 2\pi c/a$ and the smaller, higher-order band gap (3%) extends from $\omega = 0.738 \times 2\pi c/a$ to $0.763 \times 2\pi c/a$. In the subsequent sections, we will use this particular PC in order to illustrate the Wannier function approach for the accurate and efficient calculation of localized defect modes generated by simple and complex cavities, of dispersion relations for straight waveguides, and of transmission properties of PC bends.

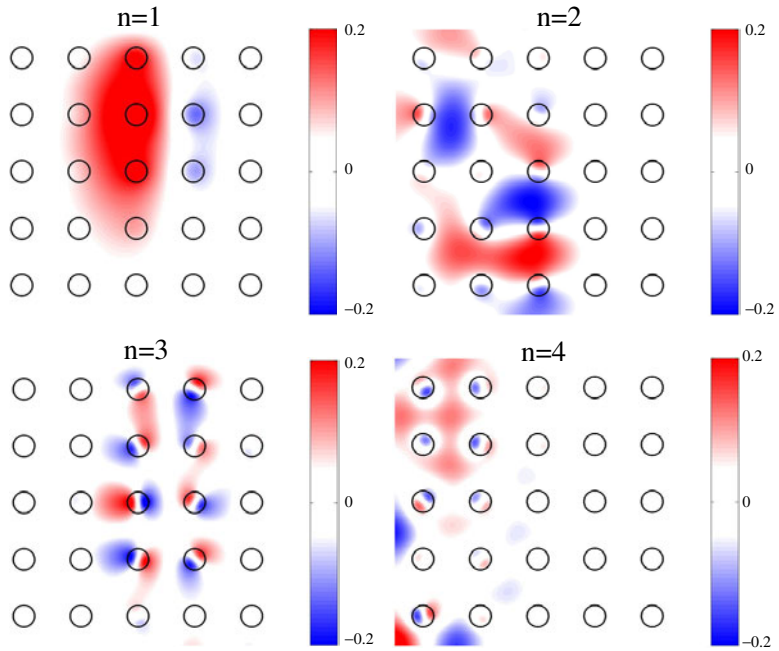

Figure 2. The photonic Wannier functions, $W_{n\vec{0}}(\vec{r})$, for the first four bands obtained by direct numerical integration of equation (4). The parameters of the underlying PC are the same as those in figure 1.

3. Maximally localized photonic Wannier functions

As discussed in the introduction, a natural description of localized defect modes associated with defect structures embedded in PCs consists of an expansion of the electromagnetic fields into an orthogonal set of localized basis functions. However, in order to obtain more physical insight into the optical properties of such defect structures, and to increase the efficiency and accuracy of the computations, it is highly desirable to encode all the relevant information such as the lattice symmetry and photonic band structure of the underlying PC, into these basis functions. Therefore, the most natural basis functions for the description of defect structures in PCs are the so-called photonic Wannier functions, $W_{n\vec{R}}(\vec{r})$, which are formally defined through a lattice Fourier transform

$$W_{n\vec{R}}(\vec{r}) = \frac{V_{\mathrm{WSC}}}{(2\pi)^2} \int_{\mathrm{BZ}} \mathrm{d}^2\vec{k}\, \mathrm{e}^{-\mathrm{i}\vec{k}\cdot\vec{R}} E_{n\vec{k}}(\vec{r}) \tag{4}$$

of the extended Bloch functions, $E_{n\vec{k}}(\vec{r})$. Here, V_{WSC} denotes the volume of the Wigner–Seitz cell (WSC). The above definition associates the photonic Wannier function $W_{n\vec{R}}(\vec{r})$ with the frequency range covered by band n, and centres it around the corresponding lattice site $\vec{R}$. In addition, the completeness and orthogonality of the Bloch functions translates directly into corresponding properties of the photonic Wannier functions

$$\int_{\mathbb{R}^2} \mathrm{d}^2\vec{r}\; W^*_{n\vec{R}}(\vec{r})\varepsilon_{\mathrm{p}}(\vec{r})W_{n'\vec{R}'}(\vec{r}) = \delta_{nn'}\delta_{\vec{R}\vec{R}'}. \tag{5}$$

Computing the Wannier functions directly from the output of photonic band-structure programs via equation (4) leads to functions with poor localization properties and erratic

behaviour (see figure 2). These problems originate from an indeterminacy of the Bloch functions. It is straightforward to show that for a group of N_W bands there exists for every wavevector $\vec{k}$ a free unitary transformation $U_{mn}(\vec{k})$ between the bands

$$E_{n\vec{k}}(\vec{r}) \rightarrow \sum_{m=1}^{N_W} U_{mn}(\vec{k}) E_{m\vec{k}}(\vec{r}), \tag{6}$$

which leaves the orthogonality relation (5) unchanged. Fixing the random part of the phases of the individual Bloch functions by requiring them to be real-valued at the origin of the WSC constitutes a simple choice of the unitary transformation $U_{mn}(\vec{k})$ and removes the erratic behaviour of the Wannier functions to a large extent. However, while being quite efficient for energetically isolated bands, this procedure fails to generate well-localized functions for energetically entangled bands. A solution to this unfortunate situation is provided by recent advances in electronic band-structure theory. Marzari and Vanderbilt [46, 60] have outlined an efficient scheme for the computation of maximally localized Wannier functions by determining numerically a transformation $U_{mn}(\vec{k})$ that minimizes an appropriate spread functional. In view of the translational properties of the Wannier functions,

$$W_{n\vec{R}}(\vec{r}) = W_{n\vec{0}}(\vec{r} - \vec{R}), \tag{7}$$

this functional reads

$$\Omega = \sum_{n=1}^{N_W} [\langle n\vec{0}|r^2|n\vec{0}\rangle - (\langle n\vec{0}|\vec{r}|n\vec{0}\rangle)^2] = \min. \tag{8}$$

Here we have introduced a shorthand notation for matrix elements according to

$$\langle n\vec{R}|f(\vec{r})|n'\vec{R}'\rangle = \int_{\mathbb{R}^2} \mathrm{d}^2\vec{r}\; W^*_{n\vec{R}}(\vec{r}) f(\vec{r}) \varepsilon_p(\vec{r}) W_{n'\vec{R}'}(\vec{r}), \tag{9}$$

for any function $f(\vec{r})$. It should be emphasized that since the unitary transformation (6) mixes the bands, the index n of the Wannier functions can no longer be referred to as a *band index*, and should be considered just as a numbering index. Nevertheless, in what follows we shall refer to it as to the *band index* implying the generalized bands [61] obtained from equation (6). In addition, we note that for an inversion-symmetric PC, $\varepsilon_p(\vec{r}) \equiv \varepsilon_p(-\vec{r})$, the Wannier functions can be chosen to be real [46].

The field distributions of the optimized Wannier functions belonging to the first six bands of our model system are depicted in figure 3. Their localization properties as well as the symmetries of the underlying PC structure are clearly visible. It should be noted that, in contrast to the case for the other bands, the Wannier centre of the second band is located halfway between the cylinders (see [46, 60] for more details on the Wannier centres). This location of the Wannier centre is a result of minimizing the spread functional, equation (8), and dramatically improves the localization properties of the second band Wannier function as compared to the case where the Wannier function centre would coincide with a cylinder site [47, 48]. Nevertheless, the orthogonality relation of the Wannier functions, equation (5), remains valid in this case. The localization properties of this set of optimized Wannier functions suggest that restricting empirical tight-binding parametrizations [31–33] or other lattice models [40] of PCs to nearest-neighbour interaction only will most likely be insufficient. More specifically, the spatial extent of the Wannier functions belonging to the first four bands of our model system (figure 3) indicate that there is small but non-negligible overlap between the Wannier functions centred on second-nearest neighbours, such that even the description of defect modes with monopole or dipole symmetry within these models might not be completely accurate using a nearest-neighbour interaction approximation. Moreover, the Wannier functions for the fifth

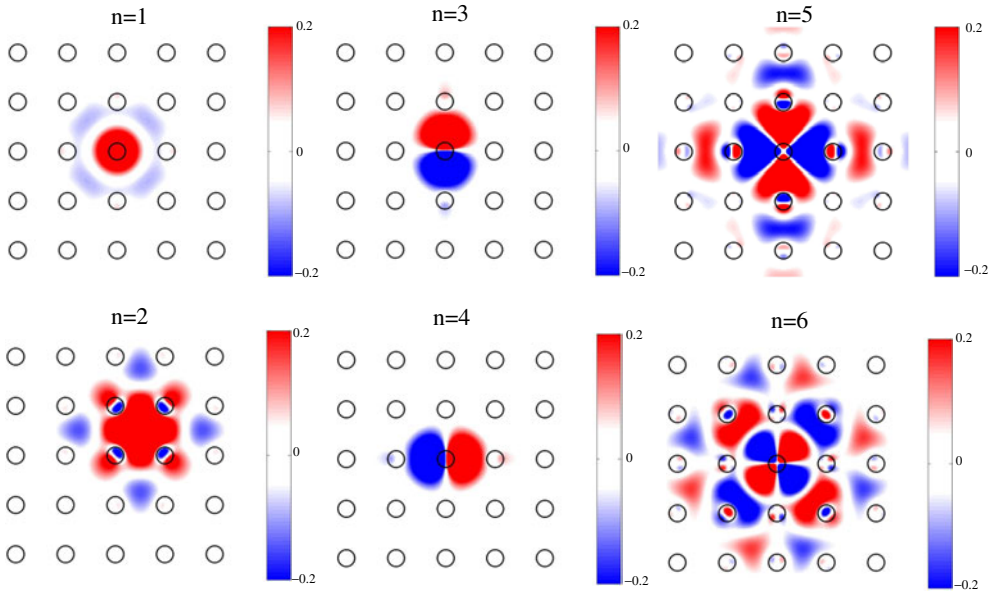

Figure 3. Photonic Wannier functions, $W_{n\vec{0}}(\vec{r})$, for the first six bands obtained by minimizing the corresponding spread functional, equation (8). Note that in contrast to the case for the other bands, the Wannier centre of the second band is located halfway between the cylinders. The parameters of the underlying PC are the same as those in figure 1.

and higher bands extend well into the unit cells adjacent to the central cell. In fact, the Wannier functions belonging to the fifth and sixth bands of our model system are predominantly localized on nearest-neighbour lattice sites and, therefore, suggest a total failure of a nearest-neighbour interaction approximation in describing localized defect modes of quadrupole symmetry.

It should be pointed out that instead of working with the electric field [47, 48], equations (1)–(5), one may equally well construct photonic Wannier functions for the magnetic field, as recently demonstrated by Whittaker and Croucher [49]. The only difference in this approach is that the weighting function $\varepsilon_{\mathrm{p}}(\vec{r})$ enters neither the orthogonality relations (3) and (5), nor the construction of matrix elements according to equation (9).

4. Defect structures in photonic crystals

Light paths for frequencies inside a PBG can be created by deliberately embedding defects into a PC. For instance, if a single rod is modified or left out altogether, an optical microcavity is formed and leads to a localized mode of light inside the PBG. A chain of such point defects can act as a linear waveguide channel and facilitate the construction of very sharp waveguide bends [62]. Combinations of these basic elements can provide ultrasmall beam splitters, Mach–Zehnder interferometers, and functional micro-optical elements such as wavelength add–drop filters. Properly designed, a set of such functional elements may allow one to realize a PC circuitry capable of guiding electromagnetic radiation in a way similar to the guidance of electrons in electronic micro-circuits. In this section, we want to illustrate—to the best of our knowledge for the first time—the usage and efficiency of the Wannier function approach in describing PC circuits by presenting within our underlying model PC a systematic study of the basic functional elements alluded to above.

The description of defect structures embedded in PCs starts with the corresponding wave equation in the frequency domain

$$\nabla^2 E(\vec{r}) + \left(\frac{\omega}{c}\right)^2 \{\varepsilon_{\mathrm{p}}(\vec{r}) + \delta\varepsilon(\vec{r})\} E(\vec{r}) = 0. \tag{10}$$

Here, we have decomposed the dielectric function into the periodic part, $\varepsilon_{\mathrm{p}}(\vec{r})$, and the contribution, $\delta\varepsilon(\vec{r})$, that describes the defect structures. Within the Wannier function approach, we expand the electromagnetic field according to

$$E(\vec{r}) = \sum_{n,\vec{R}} E_{n\vec{R}} W_{n\vec{R}}(\vec{r}), \tag{11}$$

with unknown amplitudes $E_{n\vec{R}}$. Inserting this expansion into the wave equation (10) leads to the basic equation for lattice models of defect structures embedded in PCs:

$$\sum_{n',\vec{R}'} \{\delta_{nn'}\delta_{\vec{R}\vec{R}'} + D^{nn'}_{\vec{R}\vec{R}'}\} E_{n'\vec{R}'} = \left(\frac{c}{\omega}\right)^2 \sum_{n',\vec{R}'} A^{nn'}_{\vec{R}\vec{R}'} E_{n'\vec{R}'}. \tag{12}$$

The matrix $A^{nn'}_{\vec{R}\vec{R}'}$ depends only on the dispersion relation and Wannier functions of the underlying PC and is defined through

$$A^{nn'}_{\vec{R}\vec{R}'} = \frac{V_{\mathrm{WSC}}}{(2\pi)^2} \int_{\mathrm{BZ}} \mathrm{d}^2\vec{k}\, \mathrm{e}^{\mathrm{i}\vec{k}\cdot(\vec{R}-\vec{R}')} \sum_m U^{\dagger}_{nm}(\vec{k}) \left(\frac{\omega_{m\vec{k}}}{c}\right)^2 U_{mn'}(\vec{k}). \tag{13}$$

Due to the smoothness of the photonic dispersion relation $\omega_{n\vec{k}}$ with respect to the wavevector $\vec{k}$, the exponential factor in equation (13) leads to a very rapid decay of the magnitude of matrix elements with increasing separation $|\vec{R} - \vec{R}'|$ between lattice sites, effectively making the matrix $A^{nn'}_{\vec{R}\vec{R}'}$ sparse. Furthermore, it may be shown that the matrix $A^{nn'}_{\vec{R}\vec{R}'}$ is symmetric and positive definite. Similarly, once the Wannier functions of the underlying PC are determined, the matrix $D^{nn'}_{\vec{R}\vec{R}'}$ depends solely on the overlap of these functions, mediated by the defect structure:

$$D^{nn'}_{\vec{R}\vec{R}'} = \int_{\mathbb{R}^2} \mathrm{d}^2\vec{r}\; W^*_{n\vec{R}}(\vec{r})\, \delta\varepsilon(\vec{r})\, W_{n'\vec{R}'}(\vec{r}). \tag{14}$$

As a consequence of the localization properties of both the Wannier functions and the defect dielectric function, the Hermitian matrix $D^{nn'}_{\vec{R}\vec{R}'}$, too, is sparse. Moreover, in the case of inversion-symmetric PCs, both matrices, $A^{nn'}_{\vec{R}\vec{R}'}$ and $D^{nn'}_{\vec{R}\vec{R}'}$, are real and symmetric.

Depending on the nature of the defect structure, we are interested in (i) frequencies of localized cavity modes, (ii) dispersion relations for straight waveguides, or (iii) transmission and reflection through waveguide bends and other, more complex defect structures. In the following, we consider each of these cases separately.

4.1. Localized cavity modes

As a first illustration of the Wannier function approach, we consider the case of a simple cavity created by changing the dielectric constant $\varepsilon_{\mathrm{def}}$ of a single dielectric rod at the defect site $\vec{R}_{\mathrm{def}}$ of the model PC, as shown in the inset of figure 4:

$$\delta\varepsilon(\vec{r}) = (\varepsilon_{\mathrm{def}} - \varepsilon_{\mathrm{rod}})\Theta(\vec{r} - \vec{R}_{\mathrm{def}}), \tag{15}$$

where $\Theta(\vec{r})$ defines the area of the defect rod. Specifically, $\Theta(\vec{r}) = 1$ inside a defect rod at $\vec{R}_{\mathrm{def}} = 0$ and $\Theta(\vec{r}) = 0$ outside. In this case, we directly solve equation (12) as a generalized eigenvalue problem for the cavity frequencies that lie within the PBG, and reconstruct the cavity modes from the corresponding eigenvectors.

In figure 4 we compare the frequencies of these cavity modes calculated from equation (12) with corresponding calculations using PWM-based supercell calculations [58]. Upon decreasing $\varepsilon_{\rm def}$ relative to its perfect-lattice value, a non-degenerate acceptor-like cavity mode with monopole symmetry emerges from the bottom edge of the band gap. Conversely, upon increasing $\varepsilon_{\rm def}$, doubly degenerate donor-like cavity modes of dipole symmetry emerge from the upper edge of the band gap. The results of the Wannier function approach using the $N_{\rm W} = 6$ energetically lowest-lying Wannier functions *per unit cell* in equation (12) are in complete agreement with numerically exact results of the supercell calculations. In figure 5, we depict the corresponding mode structures for a monopole cavity mode ($\varepsilon_{\rm def} = 1.0$, $\omega = 0.388 \times 2\pi c/a$, panel (a)), and for a doubly degenerate dipole cavity mode ($\varepsilon_{\rm def} = 30.0$, $\omega = 0.376 \times 2\pi c/a$, panels (b) and (c)). The symmetry properties of the cavity modes clearly correlate with the symmetry of the underlying Wannier functions. This suggests that the convergence properties of the Wannier function approach depend on the nature and symmetry properties of the cavity modes under consideration. To discuss this issue in greater detail, it is helpful to define a measure V_n of the strength of the contributions to a cavity mode from the individual Wannier function associated with band n via

$$V_n = \sum_{\vec{R}} |E_{n\vec{R}}|^2. \tag{16}$$

In figure 6, we display the dependence of the parameter V_n on the band index n for the cavity modes shown in figure 5. As expected from their respective symmetries, the dominant contributions to these cavity modes come from the Wannier functions of like symmetry. Nevertheless, the monopole cavity mode exhibits a certain (equal) contribution from the third- and fourth-band Wannier functions which exhibit dipole symmetry. Similarly, the Wannier function of the first band with monopole symmetry contributes exactly the same amount to the degenerate dipole cavity modes, whose degeneracy is further manifest in the symmetry of the contributions from the third- and fourth-band Wannier functions. Both monopole and dipole cavity modes can be completely described using the Wannier functions belonging to the six lowest bands. Therefore, we see that the frequencies of these cavity modes are already fully converged when working with only six Wannier functions per unit cell (for a comparison with numerically exact supercell calculations, see figure 4). We confirmed this result by systematically incorporating up to 20 Wannier functions. However, this situation might be quite different for other types of cavity mode. For instance, an analysis of the V_n-parameter shows that an accurate description of quadrupole cavity modes which occur for very large values of the defect dielectric constant, $\varepsilon_{\rm def} \approx 100.0$, should incorporate the Wannier functions of bands 5 and 10. Similarly, accurate results for dipole cavity modes created by increasing the radius of the defect rod requires the incorporation of the Wannier functions associated with bands 8–10 and 13–17.

Another important issue within the Wannier function approach is the question of how many lattice sites should be retained in a numerical implementation of the expansion (11). In figure 7 we display the contributions $E_{n\vec{R}}$ from individual lattice sites $\vec{R}$ to the monopole cavity mode (see figure 5(a)) for the first four bands. These contributions decay very rapidly with increasing distance $d = |\vec{R} - \vec{R}_{\rm def}|$ of the lattice site $\vec{R}$ from the defect site $\vec{R}_{\rm def}$. In particular, once this separation exceeds three lattice constants, i.e., $d > 3a$, the corresponding contributions are negligibly small. We have confirmed this result by systematically incorporating all lattice sites up to a separation of seven lattice constants. Similar results hold for other cavity modes of dipole and quadrupole symmetry. This (i) suggests that the Wannier function approach leads generically to computational tasks which involve only sparse matrices and (ii) further highlights the inadequacy of the nearest-neighbour interaction approximation.

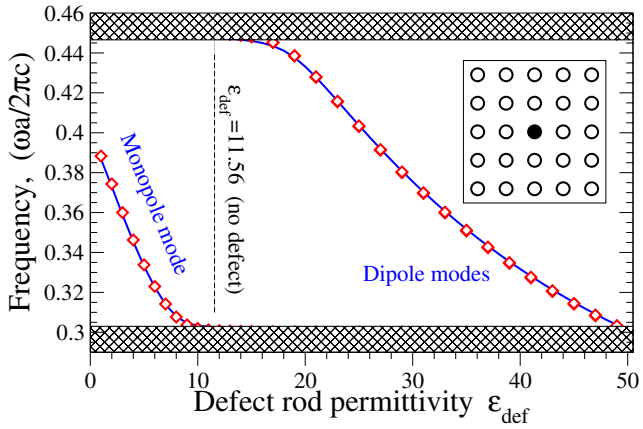

Figure 4. Frequencies of localized cavity modes associated with a single defect rod with dielectric constant $\varepsilon_{\rm def}$ (see the inset). The results of the Wannier function approach (diamonds) using $N_{\rm W} = 6$ Wannier functions per unit cell in equation (12) are in complete agreement with numerically exact results of the supercell calculations (full curves). The parameters of the underlying PC are the same as those in figure 1. See also figure 5 for the mode structure of these modes.

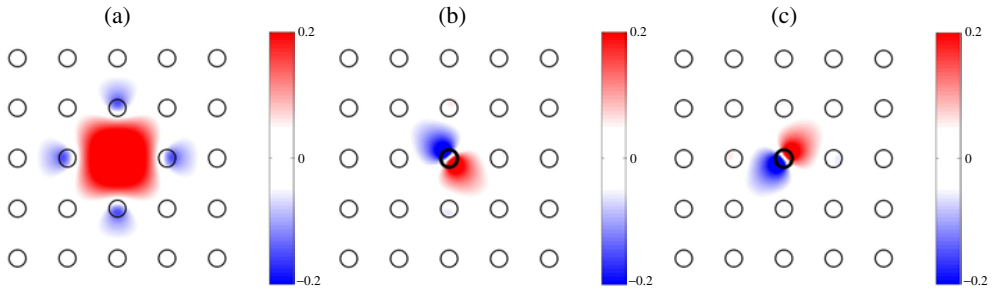

Figure 5. Localized cavity modes associated with a single defect rod: (a) removing one rod, $\varepsilon_{\rm def} = 1.0$, leads to the formation of a non-degenerate monopole cavity mode ($\omega = 0.388 \times 2\pi c/a$), whereas ((b), (c)) increasing the dielectric constant of the defect rod, $\varepsilon_{\rm def} = 30.0$, leads to the formation of a doubly degenerate dipole cavity mode ($\omega = 0.376 \times 2\pi c/a$). These results are calculated from equation (12) with $N_{\rm W} = 6$ Wannier functions per unit cell. The parameters of the underlying PC are the same as those in figure 1.

The efficiency of the Wannier function approach is particularly evident when considering defect clusters consisting of several defect rods. Since the creation of defects with prescribed dielectric constants represents a major challenge for material synthesis, such defect clusters offer an alternative route to creating cavity modes with prescribed frequencies and symmetries. As an illustration, we consider a system of four defects whose defect dielectric function, $\delta\varepsilon(\vec{r})$, can be written as sum over certain lattice sites:

$$\delta\varepsilon(\vec{r}) = \sum_m (\varepsilon_m - \varepsilon_{\rm rod})\Theta(\vec{r} - \vec{R}_m), \tag{17}$$

where $\vec{R}_m$ and ε_m denote the position and the dielectric constant of the mth defect, respectively. In this case equation (14) reduces to a sum,

$$D^{nn'}_{\vec{R}\vec{R}'} = \sum_m (\varepsilon_m - \varepsilon_{\rm rod}) B^{nn'}_{\vec{R}-\vec{R}_m, \vec{R}'-\vec{R}_m}, \tag{18}$$

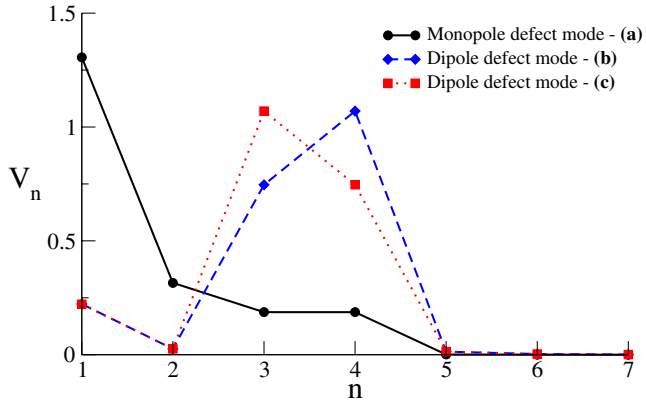

Figure 6. The strength V_n of the individual contributions from the Wannier functions of the lowest seven bands (index n) to the formation of the cavity modes depicted in figure 5. The parameters of the underlying PC are the same as those in figure 1.

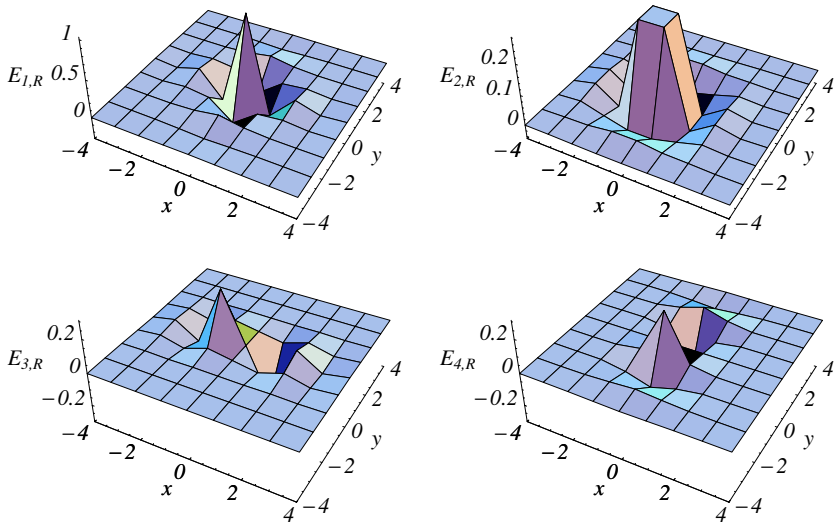

Figure 7. Contributions $E_{n\vec{R}}$ from individual lattice sites $\vec{R}$ to the monopole cavity mode displayed in figure 5(a) for the first four bands ($n = 1, 2, 3, 4$). The parameters of the underlying PC are the same as those in figure 1.

over the matrix elements

$$B^{nn'}_{\vec{R}\vec{R}'} = \int_{\mathbb{R}^2} \mathrm{d}^2\vec{r}\; W^*_{n\vec{R}}(\vec{r})\Theta(\vec{r})W_{n'\vec{R}'}(\vec{r}), \tag{19}$$

for a single defect rod situated at the point $\vec{R} = 0$. As a consequence, equation (12) takes on the form

$$\sum_{n',\vec{R}'}\left\{\delta_{nn'}\delta_{\vec{R}\vec{R}'} + \sum_m(\varepsilon_m - \varepsilon_{\mathrm{rod}})B^{nn'}_{\vec{R}-\vec{R}_m,\vec{R}'-\vec{R}_m}\right\}E_{n'\vec{R}'} = \left(\frac{c}{\omega}\right)^2\sum_{n',\vec{R}'}A^{nn'}_{\vec{R}\vec{R}'}E_{n'\vec{R}'}. \tag{20}$$

In figure 8, we display the frequencies of the localized modes generated by a defect cluster consisting of four defect rods with identical dielectric constants, $\varepsilon_m \equiv \varepsilon_{\mathrm{def}}, m = 1, 2, 3, 4$,

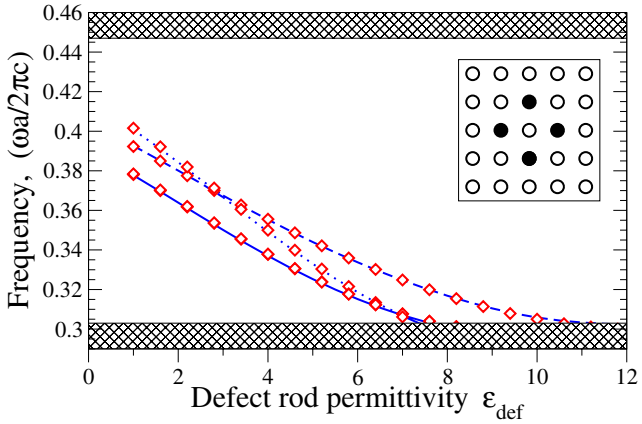

Figure 8. Frequencies of localized cavity modes for a cluster consisting of four identical defect rods with dielectric constant $\varepsilon_{\mathrm{def}}$. The positions of the defect rods are shown as black circles in the inset. The results of the Wannier function approach ($N_{\mathrm{W}} = 6$, diamonds) are in complete agreement with supercell calculations for the double degenerate dipole cavity mode (solid curve), the second-order monopole cavity mode (dashed curve), and the quadrupole cavity mode (dotted curve). The parameters of the underlying PC are the same as those in figure 1.

as functions of $\varepsilon_{\mathrm{def}}$. The positions of the defect rods are shown as black circles in the inset of figure 8. Similarly to the case of a single defect rod, the results of the Wannier function calculations are in complete agreement with plane-wave-based supercell calculations. However, we would like to emphasize that the Wannier function calculations require only little more numerical effort as compared to the calculations for a single rod. In fact, the Wannier function calculations scale linearly with the number of sites considered. More important, however, is the fact that owing to the translational properties (7) of the Wannier functions, the computation of the present defect cluster requires only the computation of matrix elements (19) for a single defect rod, which are subsequently assembled according to equation (18). Therefore, for a given underlying PC structure, it becomes possible to build up a database of matrix elements, equation (19), for different geometries of defect rods, which would allow highly efficient defect computations through simple matrix assembly procedures. This is in stark contrast to *any* other computational technique known to us.

4.2. Dispersion relations of waveguides

Arguably the most important types of defect clusters in PCs are one or several adjacent straight rows of defects. Properly designed, such defect rows form a PC waveguide which allows the efficient guiding of light for frequencies within a PBG [62, 63]. Due to the one-dimensional periodicity of such a waveguide, its guided modes obey the 1D Bloch–Floquet theorem

$$E(\vec{r} + \vec{s}_{\mathrm{w}}) = \mathrm{e}^{\mathrm{i}\vec{k}(\omega)\cdot\vec{s}_{\mathrm{w}}} E(\vec{r}) \tag{21}$$

and thus they can be labelled by a wavevector, $\vec{k}(\omega)$, parallel to the waveguide director, $\vec{s}_{\mathrm{w}} = w_1\vec{a}_1 + w_2\vec{a}_2$, where $\vec{a}_1 = (a, 0)$ and $\vec{a}_2 = (0, a)$ are the primitive lattice vectors of the PC, and integers w_1 and w_2 define the direction of the waveguide (for instance, an x-axis-directed W1 waveguide is described through $w_1 = 1$ and $w_2 = 0$). Commonly, investigations of PC waveguides consist of calculations of the dispersion relations, $\vec{k}(\omega)$, of all the guided modes. In this section we show how they can be calculated with the Wannier function approach.

As an illustration, we consider an infinite W1 waveguide consisting of a single row of identical defect rods with dielectric constant $\varepsilon_{\mathrm{def}}$:

$$\delta\varepsilon(\vec{r}) = \sum_{m=-\infty}^{\infty} (\varepsilon_{\mathrm{def}} - \varepsilon_{\mathrm{rod}})\Theta(\vec{r} - \vec{R}_m), \tag{22}$$

where the positions $\vec{R}_m = \vec{R}_0 + m\vec{s}_{\mathrm{w}}$ of the defect rods are described through the waveguide director, $\vec{s}_{\mathrm{w}}$, and the origin of the waveguide, $\vec{R}_0$. Waveguides with several adjacent defect rows (correspondingly called W2, W3 waveguides, etc) may be defined in a similar fashion. It is convenient now to rewrite equation (20) as

$$\sum_{n'\vec{R}'} M^{nn'}_{\vec{R}\vec{R}'}(\omega) E_{n'\vec{R}'} = 0 \qquad \forall n \text{ and } \vec{R}, \tag{23}$$

where the coefficients

$$M^{nn'}_{\vec{R}\vec{R}'} = \delta_{nn'}\delta_{\vec{R}\vec{R}'} + (\varepsilon_{\mathrm{def}} - \varepsilon_{\mathrm{rod}}) \sum_{m=-\infty}^{\infty} B^{nn'}_{\vec{R}-\vec{R}_m, \vec{R}'-\vec{R}_m} - \left(\frac{c}{\omega}\right)^2 A^{nn'}_{\vec{R}\vec{R}'} \tag{24}$$

exhibit periodicity along the waveguide axis:

$$M^{nn'}_{\vec{R}-\vec{s}_{\mathrm{w}}, \vec{R}'-\vec{s}_{\mathrm{w}}} = M^{nn'}_{\vec{R}\vec{R}'} \qquad \forall \vec{R} \text{ and } \vec{R}'. \tag{25}$$

To calculate the waveguide dispersion relation we combine equation (23) with the Bloch–Floquet theorem for the waveguide modes, equation (21). This is facilitated by partitioning the expansion coefficients $E_{n\vec{R}}$ into identical slices perpendicular to the waveguide that contain exactly one structural unit of the waveguide. This partitioning is analogous to the definition of a supercell and is illustrated in figure 9 for a W1 waveguide along the x-axis. As a consequence, this partitioning induces vectors $\vec{\mathcal{E}}_i = \{E_{n,\vec{\rho}_i}\}$ that consist of the amplitudes of all Wannier functions ($n = 1, 2, \ldots, N_{\mathrm{W}}$) that are centred around lattice sites $\vec{\rho}_i$ contained in slice i whose structural unit is located at site $\vec{R}_i = \vec{R}_0 + \mathrm{i}\vec{s}_{\mathrm{w}}$. A corresponding partitioning of the matrix $M^{nn'}_{\vec{R}\vec{R}'}$ in equation (24) leads to the introduction of submatrices $\hat{\mathcal{M}}_{i,j} \equiv \hat{\mathcal{M}}_{i-j}$ that describe the coupling of different slices. In a numerical implementation, these infinite submatrices $\hat{\mathcal{M}}_{i,j}$ are truncated by taking into account only a finite number of bands, N_{W}, and a finite number of lattice sites, N_{R}, surrounding defect rods inside each slice, for which the coupling of Wannier functions is relevant. Then, the matrices $\hat{\mathcal{M}}_{i,j}$ acquire the dimension $(N_{\mathrm{R}}N_{\mathrm{W}}) \times (N_{\mathrm{R}}N_{\mathrm{W}})$. Assuming that the coupling between slices separated by the distance exceeding La can be neglected, i.e., $\hat{\mathcal{M}}_{i-j} \equiv 0$ for $|\vec{R}_i - \vec{R}_j| \geqslant La$, we finally arrive at (instead of equation (23)) the matrix equation

$$\sum_{j=i-L}^{i+L} \hat{\mathcal{M}}_{i-j}\vec{\mathcal{E}}_j = 0, \tag{26}$$

which can be rewritten, generalizing the approach of [41, 53], in a transfer matrix form by defining the composite vectors $\vec{F}_i = \{\vec{\mathcal{E}}_i, \vec{\mathcal{E}}_{i+1}, \ldots, \vec{\mathcal{E}}_{i+2L-1}\}$. As a result, we obtain

$$\vec{F}_{i-1} = \hat{T}(\omega)\vec{F}_i, \tag{27}$$

where the transfer matrix $\hat{T}(\omega) = \{\hat{T}_{i,j}(\omega)\}$ has non-zero submatrix entries only for

$$\begin{aligned} &\hat{T}_{1,j}(\omega) = -\hat{\mathcal{M}}_L^{-1}(\omega)\hat{\mathcal{M}}_{L-j}(\omega) \qquad \text{for } j = 1, 2, \ldots, 2L, \\ &\hat{T}_{j+1,j} = 1 \qquad \text{for } j = 1, 2, \ldots, 2L-1. \end{aligned} \tag{28}$$

Combining equation (27) with the Bloch–Floquet theorem (21) allows us to identify the waveguide dispersion relations as the set of transfer matrix eigenvalues

$$\hat{T}(\omega)\vec{\Phi}^{(p)}(\omega) = \exp\{\mathrm{i}k_{\mathrm{p}}(\omega)s_{\mathrm{w}}\}\vec{\Phi}^{(p)}(\omega). \tag{29}$$

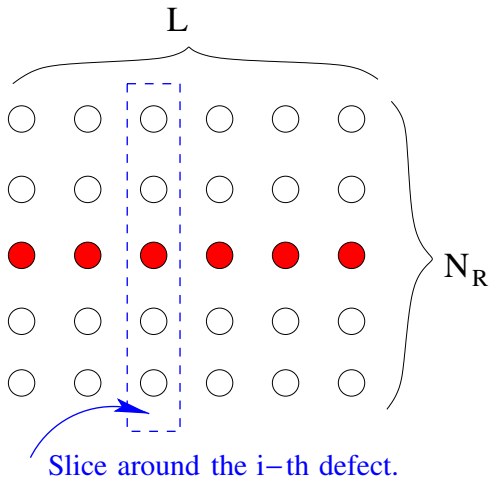

Figure 9. A PC with embedded waveguide structure can be partitioned into identical computational slices (supercells) that contain exactly one structural unit of the waveguide. This partitioning facilitates the definition of a transfer matrix, equation (27), on the basis of equation (23). In addition, we indicate the number, N_R, of lattice sites inside one slice and the number, L, of interacting slices which are taken into account in the electric field expansion.

Here, $\vec{\Phi}^{(p)}(\omega)$, $p = 1, \ldots, 2N_R N_W L$ represents the particular guided mode associated with the wavevector $k_p(\omega)$. By construction, the real part of all such wavevectors may be restricted to lying within the reduced BZ defined through $|\mathrm{Re}[k_p]| \leqslant \pi/s_w$. In figure 10(a) we plot as an example the wavevectors $k_p(\omega)$ at $\omega = 0.42 \times 2\pi c/a$ for the guided modes of a single-mode PC waveguide created by removing a row of rods. In addition to the *propagating* guided modes with real wavevectors $k_p(\omega)$, any waveguide supports a multitude of *evanescent* guided modes with complex wavevectors $k_p(\omega)$ which decay or grow slowly (with $\mathrm{Im}[k_p] \simeq \pm a^{-1}$) along the waveguide. Their significance will be discussed in sections 4.3 and 5.

To date, investigations of straight PC waveguides have concentrated on the calculation of dispersion relations for *propagating guided modes only*. Such calculations can be accurately carried out by employing the supercell technique. In figures 10(b) and 11 we display the dispersion relations for propagating guided modes for a number of different waveguide types calculated within the Wannier function approach, equation (29). The results of these calculations, using $N_R = 7$, $L = 5$, and the six energetically lowest-lying Wannier functions, are fully converged and in complete agreement with the results of plane-wave-based supercell computations. Similar to the calculations of complex cavity structures, the calculations within the Wannier function approach require fairly minimal computational resources in comparison with the supercell technique. In contrast to the recently developed effective discrete equation approach [41, 53], the Wannier function approach remains accurate even in the vicinity of band edges for the waveguides formed by chains of monopole cavity modes (see figures 10(b) and 11(a)). Similarly, the Wannier function approach can be used for investigations of PC waveguides formed by chains of doubly degenerate dipole cavity modes (see figure 11(b)) and other higher-order cavity modes.

We would like to emphasize that, in contrast to the supercell technique, the Wannier function approach, equation (29), enables us to also obtain the dispersion relations for *evanescent* guided modes (see figure 10(a)). Clearly, these modes are largely irrelevant in perfectly periodic straight waveguides. However, they do play an important role as soon

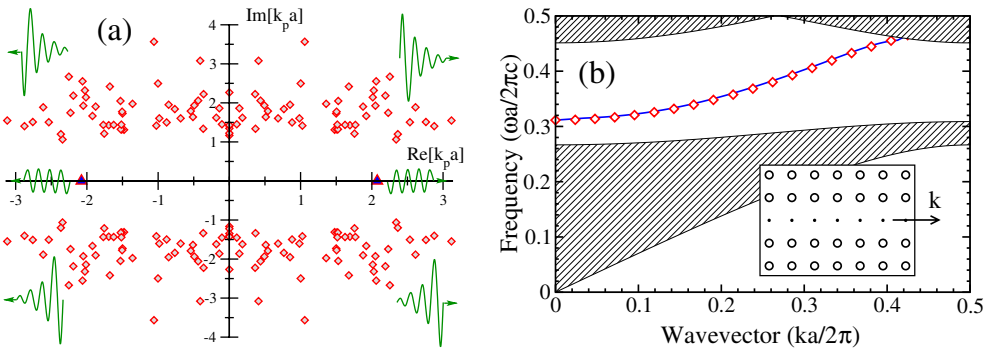

Figure 10. (a) Complex wavevectors $k_p(\omega)$ at $\omega = 0.42 \times 2\pi c/a$ for the guided modes of a PC waveguide consisting of a missing row of rods in the underlying PC, calculated within the Wannier function approach, equation (29), using $N_R = 7$, $L = 5$, and the $N_W = 6$ energetically lowest-lying Wannier functions. Notice the existence of two *propagating* guided modes (triangles pointing up) with real $k_p(\omega)$ and a multitude of slowly decaying and growing *evanescent* guided modes (diamonds) with complex $k_p(\omega)$. The totality of these modes facilitates the *complete* characterization of the waveguide through a scattering matrix as discussed in sections 4.3 and 5. (b) The dispersion relation of the propagating guided mode with $k_p(\omega) > 0$ for the same PC waveguide. This W1 waveguide may be regarded as a chain of monopole cavity modes (see figure 5(a)) leading to a single waveguide mode with even symmetry. The calculations within the Wannier function approach (diamonds) are in complete agreement with the results of supercell calculations (solid curve). The grey areas represent the projected band structure of the underlying PC whose parameters are the same as those in figure 1.

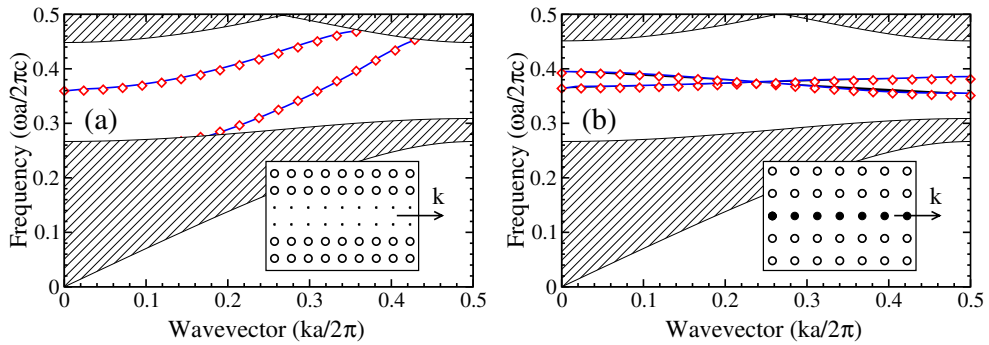

Figure 11. Dispersion relations of the propagating guided modes for PC waveguides consisting: (a) of two missing rows of rods in the underlying PC—this W2 waveguide may be regarded as two coupled chains of monopole cavity modes (see figure 5(a)) leading to two waveguide mode branches with even and odd symmetry; (b) of a row of identical rods whose dielectric constants $\varepsilon_{def} = 30.0$ have been modified from the $\varepsilon_{rod} = 11.56$ of the underlying PC—this W1 waveguide may be regarded as a chain of doubly degenerate dipole cavity modes (see figures 5(b), (c)) leading to two waveguide mode branches with even and odd symmetry. The calculations within the Wannier function approach, equation (29), using $N_R = 7$, $L = 5$, and the $N_W = 6$ energetically lowest-lying Wannier functions (diamonds), are in complete agreement with the results of supercell calculations (solid curves). The grey areas represent the projected band structure of the underlying PC whose parameters are the same as those in figure 1. The dots (black circles) in the insets indicate the lattice sites of the missing (modified) rods.

as the perfect periodicity of the waveguide is broken either through imperfections due to fabricational tolerances, or through the deliberate creation of deviations from periodicity such as bends or coupled cavity-waveguide systems for wavelength-division multiplexing (WDM)

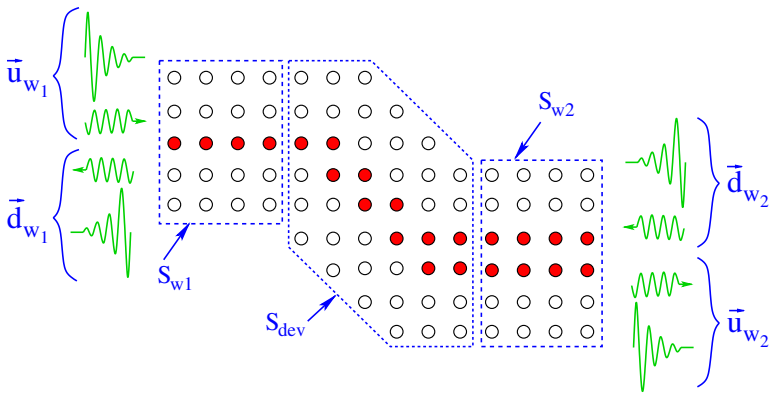

Figure 12. A defect structure (filled circles) embedded into a PC (open circles) representing a two-port device which consists of the actual device, indicated by the central polygon, with attached waveguiding leads. The leads, too, may be regarded as two-port devices as indicated by the corresponding rectangles. The central polygon and the rectangles delineate all lattice sites which are taken into account within the Wannier function approach using $N_R = 5$ and $L = 2$ (see figure 9 for the details). The Wannier function approach facilitates the *complete* characterization of these devices through the calculation of appropriate scattering matrices of individual PC devices, S_{w1}, S_{w2}, and S_{dev}, enabling a PC circuit theory based on cascaded scattering matrices as discussed in section 5.

applications. In such cases, these *evanescent* guided modes give rise to light localization effects and determine the non-trivial transmission and reflection properties of PC circuits [41, 53] as we will discuss below.

4.3. Light propagation through photonic crystal circuits

As alluded to earlier, PCs with embedded defects, such as microcavities and waveguiding structures, hold tremendous potential for the creation of photonic integrated circuits. Recent experimental attempts to fabricate the simplest types of PC-based optical circuit are, indeed, very promising [64]. Until now, the transmission properties of PC circuits were mostly studied using various implementations of the FDTD methodology. While this is a perfectly legitimate approach, which rests on some 30 years of experience, this technique does require substantial computational resources and, as a consequence, modelling has been restricted to selected small-scale PC circuits. Moreover, certain computationally intensive aspects related to small-scale PC circuits such as studies of the effect of fabricational tolerances and the optimization of device designs still present serious challenges when working with FDTD methods. In the following, we will demonstrate that the Wannier function approach provides an efficient simulation tool for the description of light propagation through PC circuits which allows one to overcome most of these limitations.

As an illustration, we consider light propagation through two-port PC circuits such as waveguide bends or coupled cavity-waveguide systems. The common feature of these devices is that two semi-infinite straight PC waveguides act as leads that are connected through a finite-sized region of defects. In figure 12, we have illustrated this principle for a double bend connecting PC waveguides of two different types. In this case, light propagation through the device at frequency ω is governed by equation (23), which should be truncated (to obtain equal number of equations and unknowns) by prescribing certain values to the expansion coefficients, $E_{n\vec{R}}$, at some sites inside the waveguiding leads. Since these values determine the amplitudes

of the incoming light, it is physically more transparent to express the expansion coefficients $E_{n\vec{R}}$ within the leads through a superposition of the guided modes $\vec{\Phi}^{(p)}(\omega)$ with wavevectors $k_{\mathrm{p}}(\omega)$ of the corresponding infinite straight waveguide. In a numerical implementation this is facilitated by replacing the expansion coefficients $E_{n\vec{R}}$ for all lattice sites $\vec{R}$ inside each waveguiding lead, W_i, $i = 1, 2$, according to

$$\vec{F}_{\mathrm{w}_i} \equiv \{E^{\mathrm{w}_i}_{n\vec{R}}\} = \sum_{p=1}^{N} u^{(p)}_{\mathrm{w}_i}(\omega)\vec{\Phi}^{(p)}(\omega) + \sum_{p=N+1}^{2N} d^{(p)}_{\mathrm{w}_i}(\omega)\vec{\Phi}^{(p)}(\omega), \tag{30}$$

where $u^{(p)}_{\mathrm{w}_i}$ and $d^{(p)}_{\mathrm{w}_i}$ are amplitudes of the guided modes, $N = N_{\mathrm{R}}N_{\mathrm{W}}L$, and we assume that all the guided modes are ordered in the following way: $p = 1$ to N are occupied by the propagating guided modes with $\mathrm{Re}[k_{\mathrm{p}}] > 0$ and evanescent guided modes with $\mathrm{Im}[k_{\mathrm{p}}] > 0$, whereas $p = N + 1$ to 2N are occupied by the propagating guided modes with $\mathrm{Re}[k_{\mathrm{p}}] < 0$ and evanescent guided modes with $\mathrm{Im}[k_{\mathrm{p}}] < 0$ (illustrated by the arrows in figure 12). Assuming that the amplitudes, $u^{(p)}_{\mathrm{w}_1}$ and $d^{(p)}_{\mathrm{w}_2}$, of all the propagating (evanescent) guided modes which propagate (decay) in the direction of the device are known (they depend on the purpose of our calculation or on the experimental set-up), we can now substitute equation (30) into (23) and, solving the resulting system of coupled equations, find the unknown expansion coefficients $E_{n\vec{R}}$ for the sites $\vec{R}$ inside the domain of the device (which can be used, e.g., for visualization of the field propagation through the device), and the amplitudes, $u^{(p)}_{\mathrm{w}_2}$ and $d^{(p)}_{\mathrm{w}_1}$ of all *outgoing propagating* and *growing evanescent* guided modes.

Generally, we are interested not in the amplitudes of the guided modes but in the transmission and reflection coefficients which constitute links between incoming and outgoing waves. These coefficients can be calculated by successively varying the amplitudes of the incoming modes such that there is a unit amplitude associated with exactly one element contained in the set $\{u^{(p)}_{\mathrm{w}_1}, d^{(p)}_{\mathrm{w}_2}, p = 1, \ldots, N\}$ of incoming amplitudes. For instance, assuming that the only incoming mode j of the first waveguide has non-vanishing amplitude, we obtain from the solution of equation (23) the corresponding elements

$$t^{uu}_{ij}(\omega) = u^{(i)}_{\mathrm{w}_2}(\omega)/u^{(j)}_{\mathrm{w}_1}(\omega) \qquad \text{and} \qquad r^{du}_{ij}(\omega) = d^{(i)}_{\mathrm{w}_1}(\omega)/u^{(j)}_{\mathrm{w}_1}(\omega) \qquad \forall i \tag{31}$$

of the transmission and reflection matrices, $\hat{T}^{uu} \equiv \{t^{uu}_{ij}\}$ and $\hat{R}^{du} \equiv \{r^{du}_{ij}\}$, which describe the transmission from lead W_1 to lead W_2 and the reflection back into lead W_1, respectively. In the same way, assuming that the only incoming mode j of the second waveguide has non-vanishing amplitude, we obtain the corresponding elements

$$t^{dd}_{ij}(\omega) = d^{(i)}_{\mathrm{w}_1}(\omega)/d^{(j)}_{\mathrm{w}_2}(\omega) \qquad \text{and} \qquad r^{ud}_{ij}(\omega) = u^{(i)}_{\mathrm{w}_2}(\omega)/d^{(j)}_{\mathrm{w}_2}(\omega) \qquad \forall i \tag{32}$$

of the matrices $\hat{T}^{dd}$ and $\hat{R}^{ud}$, which describe the transmission from lead W_2 to lead W_1 and the reflection back into lead W_2, respectively.

The behaviour of the two-port device is fully characterized by its scattering matrix $\hat{S}_{\text{2-port}}$, which connects the various incoming (decaying) and outgoing (growing) modes according to

$$\begin{pmatrix} \vec{u}_{\mathrm{w}_2} \\ \vec{d}_{\mathrm{w}_1} \end{pmatrix} = \hat{S}_{\text{2-port}} \begin{pmatrix} \vec{u}_{\mathrm{w}_1} \\ \vec{d}_{\mathrm{w}_2} \end{pmatrix}, \qquad \hat{S}_{\text{2-port}} = \begin{pmatrix} \hat{T}^{uu} & \hat{R}^{ud} \\ \hat{R}^{du} & \hat{T}^{dd} \end{pmatrix}, \tag{33}$$

where we have introduced vector notation for $\vec{u}_{\mathrm{w}_i} = \{u^{(p)}_{\mathrm{w}_i}\}$ and $\vec{d}_{\mathrm{w}_i} = \{d^{(p)}_{\mathrm{w}_i}\}$. The extension of this technique to *multi-port devices* is perfectly straightforward.

In figure 13 we present the results of Wannier function calculations of the reflection spectra for different bend geometries with attached single-mode waveguide leads (see figure 10) that are embedded in our model PC. The results of the Wannier function approach using $N_{\mathrm{R}} = 5$, $L = 5$, and the $N_{\mathrm{W}} = 6$ energetically lowest-lying Wannier functions are in very good

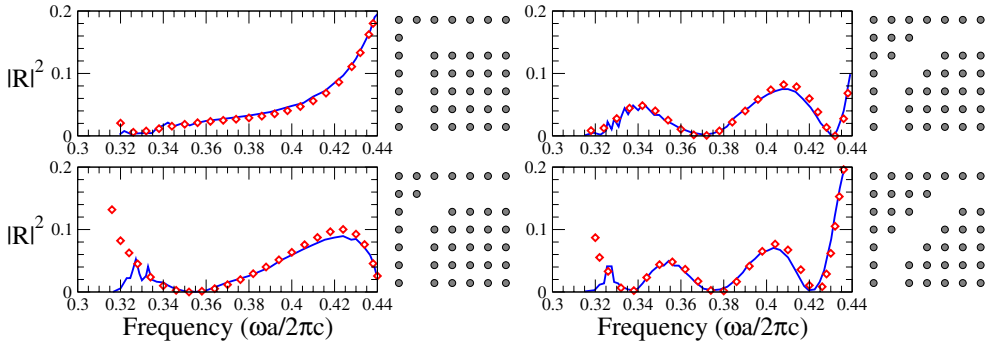

Figure 13. Reflection spectra, $|R(\omega)|^2$, for four different bend geometries embedded in a PC. The results of the Wannier function approach using $N_R = 5$, $L = 5$, and the $N_W = 6$ energetically lowest-lying Wannier functions (diamonds), are in very good agreement with the results of FDTD calculations [62] (solid curves). The parameters of the underlying PC are the same as those in figure 1.

agreement with FDTD calculations of the MIT group [62]. The deviations near the lower band edge originate in the fact that the FDTD simulations have not been carried far enough to accurately sample the signals associated with very low group velocities near the band edge.

The efficiency of the Wannier function approach for transmission calculations becomes apparent when considering that—once the *optimally localized* Wannier functions for the underlying PC have been obtained—the calculation of a single data point in the reflection spectra of figure 13 reduces to the solution of a *sparse* system of some 800 equations, which even on a laptop computer takes only a few seconds. We emphasize that even using the multiple-multipole method based on the expansion of the electric field into cylindrical harmonics (which until now has been considered as the most efficient method for 2D PCs formed by arrays of *ideally cylindrical* rods or holes) it would be necessary to solve a system of about 3265 equations (i.e., four times as large) to reach the same accuracy (see figure 9 in [51]). Perhaps more importantly and in contrast to the multiple-multipole expansion methods, the Wannier function approach can be applied to PCs with arbitrary shapes of individual scatterers.

Therefore, the Wannier function approach outlined above will

(i) enable a reverse engineering of defect structures with prescribed functionality and
(ii) allow detailed studies regarding the robustness of successful designs with respect to fabricational tolerances.

Moreover, the Wannier function approach can be straightforwardly applied, with comparable efficiency, to investigations of the transmission spectra through PC circuits made from highly dispersive and/or non-linear materials.

Of great importance is the fact that, in contrast to the FDTD method, the Wannier function approach permits one to accurately and efficiently calculate the *complete scattering matrices* (33) of PC devices. As a consequence, it provides us with the possibility to model large-scale PC devices exploiting all the advantages of a scattering matrix technique, as we discuss briefly in the next section.

5. Large-scale photonic crystal circuits

Commonly, the transmission properties of large-scale PC circuits are studied using the same methods as are used for investigations of individual PC devices (e.g., with the FDTD method).

However, when the size of a PC circuit grows significantly, even such an efficient method as the above-described Wannier function technique becomes computationally expensive.

Recently, we have demonstrated [54] that large-scale PC circuits can be very accurately described on a new level of abstraction, when considering them as systems of point-sized functional PC devices that are connected by PC waveguides. Assuming that different waveguides of a PC circuit are sufficiently far apart, one may safely neglect the cross-talk between them and one can *completely* characterize the transmission properties of functional PC devices in terms of their scattering matrices (*S*-matrices). As demonstrated in section 4.3, these *S*-matrices are expressed in terms of the guided modes of attached waveguides (see equation (33) for the case of two-port PC devices).

Within this framework, PC waveguides connecting PC devices should also be considered as two-port PC devices of special type and, therefore, should be described by the corresponding *S*-matrices. For instance, a perfect non-absorptive waveguide connector of length ℓ supporting guided modes with the dispersion relations $k_i(\omega)$, $i = 1, \ldots, 2N$, may be regarded as a perfectly transmitting and *symmetric* two-port device and, as a consequence, may be described by the diagonal *S*-matrix

$$\hat{S}_{\mathrm{w}} = \begin{pmatrix} \mathrm{e}^{\mathrm{i}k_1(\omega)\ell} & 0 & 0 \\ 0 & \cdots & 0 \\ 0 & 0 & \mathrm{e}^{\mathrm{i}k_{2N}(\omega)\ell} \end{pmatrix}. \tag{34}$$

In the case of absorptive, 2D PC slab, or disordered waveguide connectors, the *S*-matrices become more complex and should be calculated explicitly as discussed in section 4.3.

The *S*-matrix of an entire circuit consisting of many PC devices and waveguide connectors can then be calculated recursively from the *S*-matrices of the individual elements that make up the circuit [54]. In this context, we would like to emphasize the paramount importance of determining the *complete S*-matrix in terms of the *complex* transmission and reflection coefficients through equations (31), and (32). For instance, besides the intriguing properties of the reflection spectra displayed in figure 13, the waveguide bends shown in figure 13 generally exhibit a non-trivial variation in the complex phases of the transmission and reflection coefficients. These phase dependences have to be fully accounted for when describing the multiple-scattering problem of PC circuits through cascaded *S*-matrices [54].

It should be emphasized that the main difference of our scattering matrix approach from other *S*-matrix algorithms used, e.g., for modelling layered diffraction gratings [65] or small-scale integrated optics devices such as PC waveguides and air-bridge microcavities [66], consists in the choice of an *appropriate expansion basis*. In contrast to the commonly used basis of extended plane waves, *our scattering matrix approach is based on the guided modes of waveguides* attached to the PC devices under consideration. Only the incorporation of this crucial information about the underlying PC waveguides leads to *S*-matrices of low order. Moreover, key simplifications arise when the individual devices are connected through sufficiently long waveguide connectors such that their evanescent guided modes can be neglected altogether. As a consequence, the behaviour of a highly complex circuit may be described through *S*-matrices of very low order, enabling a simple and transparent PC circuit theory based on cascaded scattering matrices [54]. For instance, in the case of two-port devices with single-mode waveguide leads, the corresponding *S*-matrices are simple 2×2 matrices.

6. Conclusions

We have described a solid state theoretical approach for the calculation of the optical properties of defect structures embedded in PCs. An expansion of the electromagnetic field into photonic

Wannier functions facilitates the construction of effective lattice models which in turn allow very accurate and highly efficient computations. Once the Wannier functions for a given underlying PC have been determined, this approach requires minimal computational effort for the determination of cavity frequencies and associated mode structures, waveguide dispersion relations, and the transmission and reflection spectra of complex devices. The results of the Wannier function approach are in excellent agreement with standard techniques such as the plane-wave-based supercell method and FDTD calculations and offer considerable insight into the nature of defect modes in PCs. The efficiency and accuracy of the Wannier function approach will enable a reverse engineering of defect structures with prescribed functionality and allow the carrying out of detailed studies regarding the robustness of successful designs with respect to fabricational tolerances.

Furthermore, in contrast to the standard techniques, the Wannier function approach facilitates the *complete* characterization of defect structures through the construction of appropriate *S*-matrices. This enables a simple and transparent PC circuit theory to be based on *cascaded scattering matrices expressed in the basis of guided modes of PC waveguides* instead of the commonly used basis of plane waves. Finally, we want to mention that the Wannier function approach may easily be extended to the case of 3D PCs as well as to PC defect structures in *anisotropic*, *highly dispersive*, and *non-linear* materials.

Acknowledgments

The present work has greatly benefited from stimulating and insightful discussions with Wolfram Hergert and Peter Wölfle. Furthermore, we wish to express our gratitude to Inga Fischer for her help during the early stage of the project. This work was supported by the Centre for Functional Nanostructures (CFN) of the Deutsche Forschungsgemeinschaft (DFG) within projects A1.1 and A1.2. The research of KB and AGM is further supported by the DFG under grant Bu 1107/2-2 (Emmy-Noether programme). The work of MS is funded in the framework of the DFG Research Training Group 786 *Mixed Fields and Nonlinear Interactions* at the University of Karlsruhe.

References

[1] Yablonovitch E 1987 Inhibited spontaneous emission in solid-state physics and electronics *Phys. Rev. Lett.* **58** 2059–62

[2] John S 1987 Strong localization of photons in certain disordered dielectric superlattices *Phys. Rev. Lett.* **58** 2486–9

[3] Soukoulis C M (ed) 2001 Photonic crystals and light localization in the 21st century *Proc. NATO Advanced Study Institute on Photonic Crystals and Light Localization (Limin Hersonissou, Crete, Greece, June 2000)* (Dordrecht: Kluwer)

[4] Birner A, Wehrspohn R B, Gösele U M and Busch K 2001 Silicon-based photonic crystals *Adv. Mater.* **13** 377–88

[5] Krauss T F and De la Rue R M 1999 Photonic crystals in the optical regime—past, present and future *Prog. Quantum Electron.* **23** 51–96

[6] Forchel A, Kamp M, Happ T, Reithmaier J P, Bayer M, Koeth J and Dietrich R 2000 Photon confinement effects—from physics to applications *Microelectron. Eng.* **53** 21–8

[7] Loncar M, Doll T, Vuckovic J and Scherer A 2000 Design and fabrication of silicon photonic crystal optical waveguides *J. Lightwave Technol.* **18** 1402–11

[8] Benisty H, Olivier S, Weisbuch C, Agio M, Kafesaki M, Soukoulis C M, Qiu M, Swillo M, Karlsson A, Jaskorzynska B, Talneau A, Moosburger J, Kamp M, Forchel A, Ferrini R, Houdre R and Oesterle U 2002 Models and measurements for the transmission of submicron-width waveguide bends defined in two-dimensional photonic crystals *IEEE J. Quantum Electron.* **38** 770–85

[9] Noda S, Imada M, Chutinan A and Yamamoto N 2002 III–V-based semiconductor photonic crystals *Opt. Quantum Electron.* **34** 723–36
[10] Liguda C, Böttger G, Kuligk A, Blum R, Eich M, Roth H, Kunert J, Morgenroth W, Elsner H and Meyer H G 2001 Polymer photonic crystal slab waveguides *Appl. Phys. Lett.* **78** 2434–6
[11] Edrington A C, Urbas A M, DeRege P, Chen C X, Swager T M, Hadjichristidis N, Xenidou M, Fetters L J, Joannopoulos J D, Fink Y and Thomas E L 2001 Polymer-based photonic crystals *Adv. Mater.* **13** 421–5
[12] Schueller O J A, Whitesides G M, Rogers J A, Meier M and Dodabalapur A 1999 Fabrication of photonic crystal lasers by nanomolding of solgel glasses *Appl. Opt.* **38** 5799–802
[13] Rosenberg A, Tonucci R J, Lin H B and Shirley E L 1996 Photonic-band-structure effects for low-index-contrast two-dimensional lattices in the near-infrared *Phys. Rev.* B **54** R5195–8
[14] Chutinan A, John S and Toader O 2003 Diffractionless flow of light in all-optical microchips *Phys. Rev. Lett.* **90** 123901–4
[15] Lin S Y, Fleming J G, Hetherington D L, Smith B K, Biswas R, Ho K M, Sigalas M M, Zubrzycki W, Kurtz S R and Bur J 1998 A three-dimensional photonic crystal operating at infrared wavelengths *Nature* **394** 251–3
[16] Noda S, Tomoda K, Yamamoto N and Chutinan A 2000 Full three-dimensional photonic bandgap crystals at near infrared wavelengths *Science* **289** 604–6
[17] Wijnhoven J E G J and Vos W L 1998 Preparation of photonic crystals made of air spheres in titania *Science* **281** 802–4
[18] Blanco A, Chomski E, Grabtchak S, Ibisate M, John S, Leonard S W, Lopez C, Meseguer F, Miguez H, Mondia J P, Ozin G A, Toader O and van Driel H M 2000 Large-scale synthesis of a silicon photonic crystal with a complete three-dimensional bandgap near 1.5 micrometres *Nature* **405** 437–40
[19] Vlasov Y A, Bo X Z, Sturm J C and Norris D J 2001 On-chip natural assembly of silicon photonic bandgap crystals *Nature* **414** 289–93
[20] Campbell M, Sharp D N, Harrison M T, Denning R G and Turberfield A J 2000 Fabrication of photonic crystals for the visible spectrum by holographic lithography *Nature* **404** 53–6
[21] Miklyaev Y V, Meisel D C, Blanco A, von Freymann G, Busch K, Koch W, Enkrich C, Deubel M and Wegener M 2003 Three-dimensional face-centered-cubic photonic crystal templates by laser holography: fabrication, optical characterization and band-structure calculations *Appl. Phys. Lett.* **82** 1284–6
[22] Sun H B, Matsuo S and Misawa H 1999 Three-dimensional photonic crystal structures achieved with two-photon-absorption photopolymerization of resin *Appl. Phys. Lett.* **74** 786–8
[23] Sun H B, Mizeikis V, Xu Y, Juodkazis S, Ye J Y, Matsuo S and Misawa H 2001 Microcavities in polymeric photonic crystals *Appl. Phys. Lett.* **79** 1–3
[24] Straub M and Gu M 2002 Near-infrared photonic crystals with higher-order bandgaps generated by two-photon photopolymerization *Opt. Lett.* **27** 1824–6
[25] Taflove A 1988 Review of the formulation and applications of the finite-difference time-domain method for numerical modeling of electromagnetic-wave interactions with arbitrary structures *Wave Motion* **10** 547–82
[26] Fletcher C A J 1984 *Computational Galerkin Methods* (New York: Springer)
[27] Mogilevtsev D, Birks T A and Russell P S 1999 Localized function method for modeling defect modes in 2-D photonic crystals *J. Lightwave Technol.* **17** 2078–81
[28] Russell P 2003 Photonic crystal fibers *Science* **299** 358–62
[29] Monro T M, Richardson D J, Broderick N G R and Bennett P J 1999 Holey optical fibers: an efficient modal model *J. Lightwave Technol.* **17** 1093–102
[30] Ashcroft N W and Mermin N D 1976 *Solid State Physics* (New York: Saunders)
[31] Lidorikis E, Sigalas M M, Economou E N and Soukoulis C M 1998 Tight-binding parametrization for photonic band gap materials *Phys. Rev. Lett.* **81** 1405–8
[32] Albert J P, Jouanin C, Cassagne D and Bertho D 2000 Generalized Wannier function method for photonic crystals *Phys. Rev.* B **61** 4381–4
[33] Albert J P, Jouanin C, Cassagne D and Monge D 2002 Photonic crystal modelling using a tight-binding Wannier function method *Opt. Quantum Electron.* **34** 251–63
[34] Lowdin P O 1962 Band theory, valence bond and tight-binding calculations *J. Appl. Phys.* **33** 251–7
[35] Frauenheim T, Seifert G, Elstner M, Hajnal Z, Jungnickel G, Porezag D, Suhai S and Scholz R 2000 A self-consistent charge density-functional based tight-binding method for predictive materials simulations in physics, chemistry and biology *Phys. Status Solidi* b **217** 41–62
[36] Yariv A, Xu Y, Lee R K and Scherer A 1999 Coupled-resonator optical waveguide: a proposal and analysis *Opt. Lett.* **24** 711–13
[37] Xu Y, Lee R K and Yariv A 2000 Propagation and second-harmonic generation of electromagnetic waves in a coupled-resonator optical waveguide *J. Opt. Soc. Am.* B **17** 387–400

[38] Bayindir M, Temelkuran B and Ozbay E 2000 Tight-binding description of the coupled defect modes in three-dimensional photonic crystals *Phys. Rev. Lett.* **84** 2140–3
[39] Ozbay E, Bayindir M, Bulu I and Cubukcu E 2002 Investigation of localized coupled-cavity modes in two-dimensional photonic bandgap structures *IEEE J. Quantum Electron.* **38** 837–43
[40] McGurn A R 2000 Photonic crystal circuits: a theory for two- and three-dimensional networks *Phys. Rev.* B **61** 13235–49
[41] Mingaleev S F and Kivshar Y S 2002 Nonlinear transmission and light localization in photonic crystal waveguides *J. Opt. Soc. Am.* B **19** 2241–9
[42] Mingaleev S F, Kivshar Y S and Sammut R A 2000 Long-range interaction and nonlinear localized modes in photonic crystal waveguides *Phys. Rev.* E **62** 5777–82
[43] Mingaleev S F and Kivshar Y S 2001 Self-trapping and stable localized modes in nonlinear photonic crystals *Phys. Rev. Lett.* **86** 5474–7
[44] Wannier G H 1937 The structure of electronic excitation levels in insulating crystals *Phys. Rev.* **52** 191–7
[45] Leung K M 1993 Defect modes in photonic band structures: a Green's function approach using vector Wannier functions *J. Opt. Soc. Am.* B **10** 303–6
[46] Marzari N and Vanderbilt D 1997 Maximally localized generalized Wannier functions for composite energy bands *Phys. Rev.* B **56** 12847–65
[47] Garcia-Martin A, Hermann D, Busch K and Wölfle P 2002 Solid state theoretical methods for defect computations in photonic crystals *Mater. Res. Soc. Symp. Proc.* **722** L1–7
[48] Garcia-Martin A, Hermann D, Hagmann F, Busch K and Wölfle P 2003 Defect computations in photonic crystals: a solid state theoretical approach *Nanotechnology* **14** 177–83
[49] Whittaker D M and Croucher M P 2003 Maximally localized Wannier functions for photonic lattices *Phys. Rev.* B **67** 085204
[50] Asatryan A A *et al* 2001 Two-dimensional local density of states in two-dimensional photonic crystals *Opt. Express* **8** 191–6
[51] Moreno E, Erni D and Hafner C 2002 Modeling of discontinuities in photonic crystal waveguides with the multiple multipole method *Phys. Rev.* E **66** 036618
[52] Ohtaka K and Tanabe Y 1996 Photonic bands using vector spherical waves *J. Phys. Soc. Japan* **65** 2265–84
[53] Mingaleev S F and Kivshar Y S 2002 Effective equations for photonic-crystal waveguides and circuits *Opt. Lett.* **27** 231–3
[54] Mingaleev S F and Busch K 2003 Scattering matrix approach to large-scale photonic-crystal circuits *Opt. Lett.* **28** 619–21
[55] Busch K and John S 1998 Photonic band gap formation in certain self-organizing systems *Phys. Rev.* E **58** 3896–908
[56] Sipe J E 2000 Vector $k \cdot p$ approach for photonic band structures *Phys. Rev.* E **62** 5672–7
[57] Hermann D, Frank M, Busch K and Wölfle P 2001 Photonic band structure computations *Opt. Express* **8** 167–72
[58] Johnson S G and Joannopoulos J D 2001 Block-iterative frequency-domain methods for Maxwell's equations in a planewave basis *Opt. Express* **8** 173–90
[59] Busch K and John S 1999 Liquid-crystal photonic-band-gap materials: the tunable electromagnetic vacuum *Phys. Rev. Lett.* **83** 967–70
[60] Souza I, Marzari N and Vanderbilt D 2002 Maximally localized Wannier functions for entangled energy bands *Phys. Rev.* B **65** 035109
[61] Kohn W 1973 Construction of Wannier functions and applications to energy bands *Phys. Rev.* B **7** 4388–98
[62] Mekis A, Chen J C, Kurland I, Fan S H, Villeneuve P R and Joannopoulos J D 1996 High transmission through sharp bends in photonic crystal waveguides *Phys. Rev. Lett.* **77** 3787–90
[63] Joannopoulos J D, Villeneuve P R and Fan S H 1997 Photonic crystals: putting a new twist on light *Nature* **386** 143–9
[64] Krauss T and Baba T (ed) 2002 Feature section on photonic crystal structures and applications *IEEE J. Quantum Electron.* **38** 724–963
[65] Li L 1996 Formulation and comparison of two recursive matrix algorithms for modeling layered diffraction gratings *J. Opt. Soc. Am.* A **13** 1024–35
[66] Silberstein E, Lalanne Ph, Hugonin J P and Cao Q 2001 Use of grating theories in integrated optics *J. Opt. Soc. Am.* A **18** 2865–75